Surface & Coatings Technology 205 (2011) 3810–3815

Contents lists available at ScienceDirect

Surface & Coatings Technology

journal homepage: www.elsevier.com/locate/surfcoat

Structure, composition, and mechanical characterization of dc sputtered TiN-MoS_2 nanocomposite thin films

G. Strapasson [a], P.C. Badin [a], G.V. Soares [b], G. Machado [c], C.A. Figueroa [a], R. Hubler [d], A.L. Gasparin [a], I.J.R. Baumvol [a,b], C. Aguzzoli [a], E.K. Tentardini [e,*]

[a] Universidade de Caxias do Sul, Caxias do Sul, 95070-560, Brazil
[b] Instituto de Física, UFRGS, Porto Alegre, 91509-900, Brazil
[c] Centro de Tecnologia Estratégicas do Nordeste, Recife, Brazil
[d] Pontifícia Universidade Católica do Rio Grande do Sul — GEPSI, 90619-900, RS, Brazil
[e] Universidade Federal do Sergipe, Aracaju, Brazil

ARTICLE INFO

Article history:
Received 10 November 2010
Accepted in revised form 19 January 2011
Available online 26 January 2011

Keywords:
Thin films
TiN-MoS_2
Nanostructure
Nanoscopic clusters
Nanohardness
Elastic strain to failure

ABSTRACT

TiN-MoS_2 composite thin films deposited by dc magnetron sputtering with MoS_2 concentrations from 3 to 40 at.% were investigated. The elementary composition and the formed compounds were determined before and after wear. The crystalline structure of the composite thin films was accessed and the nature and concentration of the precipitates in the TiN matrix were imaged by transmission electron microscopy. The hardness and elastic moduli of the films were measured by nanoindentation and the elastic strain to failure calculated on the basis of these two magnitudes. The MoS_2 formed in the composite coatings during thin film co-deposition are nanoscopic in size, homogeneously distributed, and mostly amorphous, although part of them are crystalline. The present study does not confirm MoS_2 formation at grain boundaries or TiS formation by substitution of S for N in the TiN matrix. The hardness and elastic strain to failure are appreciably high for the present TiN-MoS_2 thin film composite coatings with MoS_2 concentrations up to 4%. The potential applications are discussed on the basis of these findings.

1. Introduction

The development of protective coatings that reduce or even eliminate the usage of liquid lubricants is a subject of current interest, since these fluids are expensive and environmentally aggressive [1–5]. Tools, moulds, and other engineering components are representative members of these applications. TiAlN coatings are currently used, as well as innovative coatings like Si_3N_4 [6–9]. Several successful cases of introducing small particles of soft lubricating material inside hard thin film matrix, retaining the coating high hardness while reducing wear and friction were described [10–13] in the literature. A specific composite, formed by incorporation of molybdenum disulfide (MoS_2) into titanium nitride (TiN) matrix is used for severe conditions of dry machining applications, as well as space and vacuum applications [14–21]. In addition to its higher hardness and load bearing capacity, TiN forms lubricious rutile transfer layer in the presence of environmental humidity. While substoichiometric, this often leads to the formation of lubricious Magneli phases. Hence, the architecture which combines both MoS_2 and TiN is expected to be hard as well as lubricious. Wear and friction coefficients were indeed substantially reduced, leading several different authors and companies to report on the potentialities of TiN-MoS_2 composite thin film coatings. In the interval of MoS_2 concentrations from zero to 7%, the friction coefficient does not depend much on the MoS_2 concentration [16].

In all routes followed to obtain such composites, TiN was the dominant phase (90–92 mol%), whereas the existence and formation conditions of a separate MoS_x phase, $1<x\leq2$, remained rather controversial. The eventual formation of MoS_2 during deposition was assumed to occur [22,23] owing to substitution of sulfur for nitrogen in the TiN lattice or, alternatively, by MoS_2 segregation at TiN grain boundaries. These observations were mainly based on X-ray diffraction (XRD) analyses, which is not an ideal technique for surface structure and composition characterizations. In addition, it was previously reported [15] the formation of MoS_2 just after mechanical wear and not during coating deposition. Finally, there is another not well clarified aspect, this one concerning the amorphous or crystalline nature of MoS_2 into the TiN matrix [24–26]. In fact, as far as we could inspect the literature, there is not a detailed investigation of the structure and chemical composition of sputter-deposited TiN-MoS_2 composite thin film coatings.

We report here on the investigation of the structure, composition, and mechanical properties of TiN-MoS_2 composite thin film coatings

* Corresponding author at: Universidade Federal do Sergipe, Núcleo de Ciência e Engenharia de Materiais, NUCEM, Av. Marechal Rondon s/n, Rosa Elze, CEP 49100-000, São Cristóvão, SE, Brazil. Tel.: +55 79 2105 6343; fax: +55 79 2105 6845.
E-mail address: etentardini@gmail.com (E.K. Tentardini).

0257-8972
doi:10.1016/j.surfcoat.2011.01.044

deposited by dc magnetron sputtering at various different concentrations of MoS_2 in the TiN matrix. The stoichiometry of the films was determined by Rutherford backscattering spectrometry (RBS). The chemical composition of the near surface regions of the films was investigated by X-ray photoelectron spectroscopy (XPS), analyzing the Mo 3d, S 2p, Ti 2p, and N 1s photoelectrons. The coating nanostructure, grain size and distributions were analyzed by transmission electron microscopy (TEM). The crystalline structure of the coatings was investigated by glancing incidence X-ray diffraction (GIXRD). The hardness and reduced elastic modulus were accessed by the nanoindentation technique with a Berkovich indenter. The hardness to Young modulus (H/E) ratio, so called elastic strain to failure, which has been proposed and consistently used to evaluate the resistance to plastic deformation of thin film coatings [27,28] was also determined. More specifically, the H^3/E^2 ratio is considered to be a good indicator of the coating resistance to wear. Thus, we determined the coating H^3/E^2 ratios, recalling that a high H^3/E^2 indicates a high resistance of the coating to plastic deformation and, presumably, a high wear resistance as well, besides of low stiffness [29–31].

2. Experimental

TiN-MoS_2 coatings were deposited by co-sputtering using dual cathode balanced magnetron sputtering with simultaneous activation of Ti and MoS_2 targets under N_2 gas environment. Target diameters were 50 mm and the target-substrate distance fixed at 120 mm.

Both targets were powered with two pulsed DC power supplies: titanium target was performed at 100 W and MoS_2 at 15 W. The difference between these two values was due to MoS_2 deposition rate be 10 times larger compared to TiN. Ar/N_2 ratio during co-deposition of Ti and MoS_2 were maintained at 70/30 using mass flow controllers. This ratio was selected based in previous deposition of pure TiN, used to obtain stoichiometric TiN thin films.

The two targets and samples are localized on the bottom and on the top of the chamber, respectively, as showed in Fig. 1. With this equipment is possible to deposit thin films up to six different deposition conditions in the same run. This is made by two moving plates localized below chamber lid. The first plate (plate 1) possesses six positions where the substrates are tied and the second plate (plate 2) has an open passage with same dimensions of substrate holder. We are able to control independently the rotation of each plate.

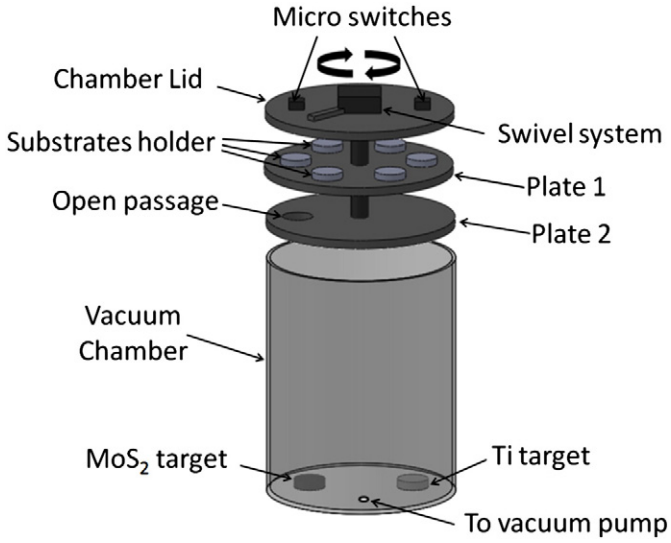

Fig. 1. Schematic representation of sputtering chamber.

Table 1
Main deposition parameters for TiN-MoS_2 composite thin films.

Power to Ti target (W)	100
Power to MoS_2 target (W)	15
Ar/N_2 ratio	70/30
Base pressure (Pa)	5×10^{-5}
Working pressure (Pa)	3×10^{-1}
Permanence time at Ti target (s)	240
Permanence time at MoS_2 target (s)	0.5 to 10
Deposition time (min)	30

To obtain TiN-MoS_2 coatings of varying composition, the substrates were positioned in all six positions in the substrate holder. The open passage was placed mechanically on the desired position (1 to 6) for each run and both plates were rotated between two targets by a swivel system controlled by computer software projected specifically for this sputtering system. With micro switches localized above lid in each target position (Fig. 1), it was possible to control the substrate time dwelling on each target position and the total deposition time, allowing the formation of TiN-MoS_2 coatings with different MoS_2 amounts.

Pure carbon substrates were used for RBS analyses, silicon substrates for XPS, GIXRD and nanoindentation, and polymer substrates for TEM analyses.

Prior to deposition, all substrates undergone ultrasonic cleaning in acetone, followed by a deionized water bath, and finally dried with pure nitrogen. All deposition parameters were kept constant, with the exception of substrate dwelling time on the MoS_2 target. Table 1 summarizes the main deposition parameters.

MoS_2/TiN ratios were determined by Rutherford Backscattering Spectroscopy (RBS) [32] using a 2 MeV He^+ beam at normal incidence and a backscattering detection angle of 165°. The areal densities of all chemical species were determined with 5 to 10% accuracy using a Sb-implanted silicon standard.

The GIXRD analyses were performed with a Shimadzu XRD-2000 equipment, using Cu-Kα radiation, incidence angle of 1° and scans from 10 to 90° in 0.05 steps.

XPS analyses were performed in an Omicron SPHERA station using Mg-K_α radiation (1253.6 eV) at a take-off angle of 45° with an energy resolution of 0.9 eV. In order to identify the constituents of the coatings, we have performed a systematic deconvolution of the S 2p, Mo 3d, Ti 2p and N 1s bands as a function of oxygen content. The spectra deconvolution uses symmetrical peak type *PsdVoigt1* (Gaussian and Lorenz contribution) with a fixed energy maximum and a variable FWHM between 1 and 2.5 eV.

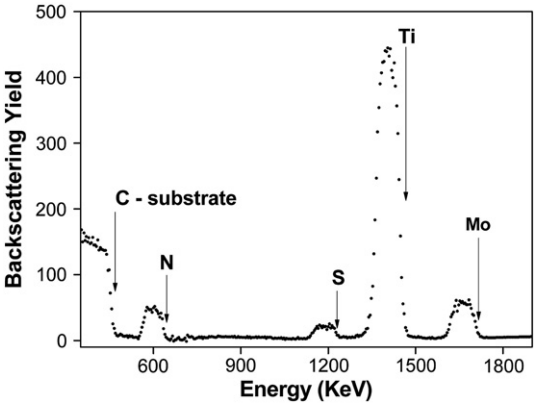

Fig. 2. Backscattering spectra of He^+ ions incident at 2 MeV on a MoS_2-TiN composite thin film with 12% MoS_2 deposited on a C substrate (sample 3). For Mo, Ti, S, and N the arrows indicate the backscattering energies from the corresponding elements at the film surface, whereas for C, the arrow indicates the backscattering energy corresponding to C at the film-substrate interface.

Table 2
Permanence time at the MoS_2 target and MoS_2/TiN ratios in the TiN-MoS_2 composite thin films.

Sample	Permanence time at MoS_2 target (s)	MoS_2/TiN
1	0.5	0.030
2	1	0.043
3	3	0.120
4	5	0.190
5	7	0.281
6	10	0.403

TEM images were obtained in the following way. The thin film TiN-MoS_2 films deposited on polymer were embedded in an epoxy resin and cured at 50 °C for 72 h. The embedded specimens were first trimmed with a razor blade and then an ultra-thin cut was carried out with a 35° Diatome diamond knife. The samples were microtomed in 70 nm thick slices and mounted on 200 mesh copper grids. Finally, they were examined using a FEI, Morgagni 268D microscope operating at an accelerating voltage of 80 kV.

The nanoidentation measurements were performed with a NanoTest 600 from Micro Materials Ltds., at a load rate of 0.06 N s^{-1} and a maximum indentation depth of 50 nm.

All samples were characterized as deposited by the above described techniques and by RBS, XPS and GIXRD after dry wear simulations for variable times. Samples were submitted to mechanical wear in a pin-on-disk system adapted specifically to evaluate thin films samples. In this system, a 150 mm diameter metal disc with a DP-MOL polished pad composed by a homogeneous suspension of 1% diamond (1 μm granulometry) is disperse in a ethylene glycol/isopropyl alcohol (1:1) solution. The "pin" is formed by the thin film sample with 1 cm^2 area tied in a fixed arm in a distance of 50 mm from disc center and stuck against the disc with a normal force of 25 N, producing a pressure of 0.25 MPa. To avoid sample heating, samples were submitted to a total of 1000 cycles in this condition, corresponding a covered distance of 314 m with radial speed of 0.8 m/s (153 rpm). This process produces a mechanical wear between 70 to 90 nm, around one third of the composite films. Measurements were made at room temperature of 25° C.

3. Results and discussion

A typical RBS spectrum is shown in Fig. 2, as obtained from sample 3. The carbon substrate was used for RBS analyses in order to eliminate the high background signal from Si, which is commonly used as substrate. Similar spectra (not shown) were obtained for the other TiN/MoS_2/C samples. Table 2 gives the MoS_2/TiN ratios as determined by RBS, numbering the samples from 1 to 6 (herein used to identify the samples) by order of increasing MoS_2/TiN ratio. The N/Ti and S/Mo ratios were also determined by RBS as being 1.1 ± 0.1 and 1.9 ± 0.2, respectively.

The projected thickness of the composite films were 250 nm for samples deposited on silicon and carbon substrates and 100 nm for samples deposited on polymeric substrates, which were used for TEM analyses. However, RBS analyses indicated variations in the film thickness as the MoS_2 concentration increases.

Fig. 3a shows the Mo 3d photoelectron regions, as obtained from sample 2 before and after wear. The two doublet components at binding energies of 229.5 eV and 232.2 eV (Mo $3d_{5/2}$) are assigned to MoS_2 and Mo–O–S bonds [3,16], respectively. The corresponding S 2p photoelectron regions for the same samples are shown in Fig. 3b. The components at binding energies of 161.8 eV and 163.7 eV (S $2p_{3/2}$) can be assigned to MoS_2 [3,12] and MoS_{2-x}, respectively. The component at a binding energy of 168.9 eV can be assigned to S–O–Mo bonds [33]. The Ti 2p photoelectron regions are presented in

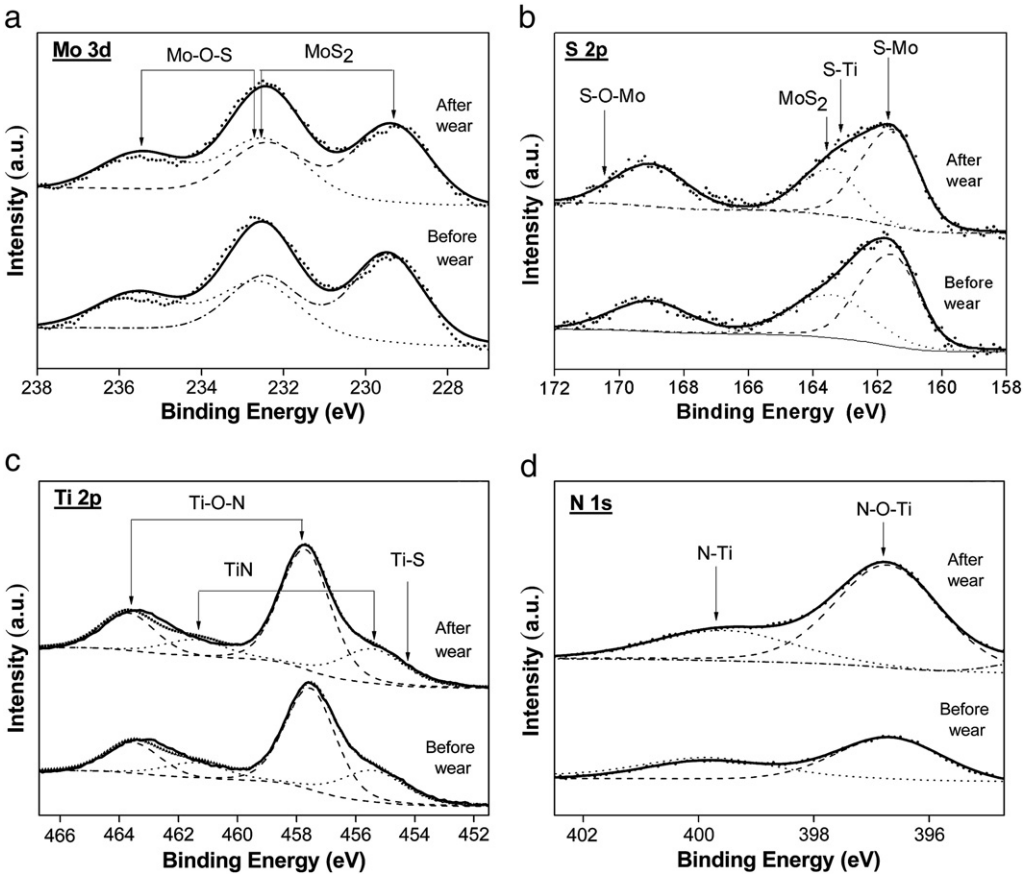

Fig. 3. X-ray photoelectron spectroscopy regions for (a) Mo 3d, (b) S 2p, (c) Ti 2p, and (d) N 1s. The components used in the simulations are indicated in the figures.

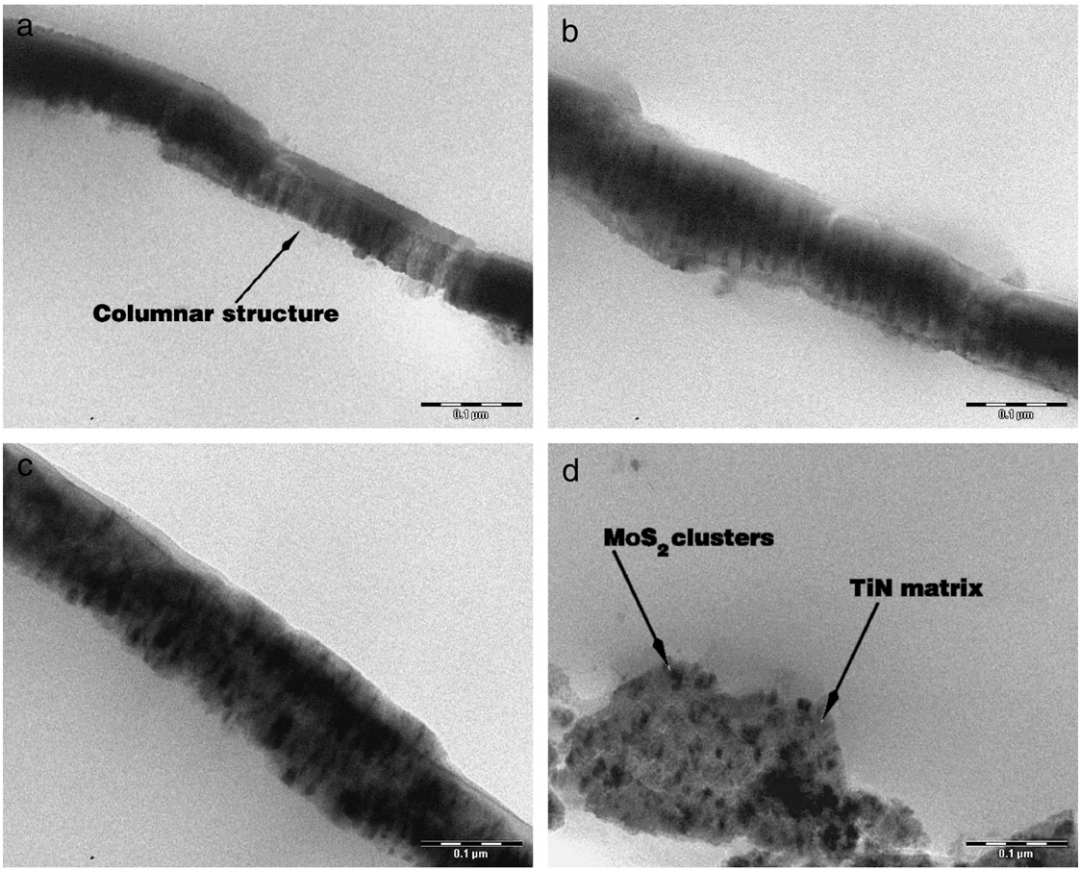

Fig. 4. Transmission electron microscopy images for TiN-MoS_2 composite thin films: (a) 4.3% MoS_2 (b) 12% MoS_2 (c) 19% MoS_2 (d) 28% MoS_2.

Fig. 3c, evidencing components at binding energies of 455.3 eV (Ti $2p_{3/2}$) assigned to TiN and at 457.8 eV assigned to Ti–O–N bonds in titanium oxynitrides [34]. Finally, Fig. 3d shows the N 1s photoelectron regions with peaks at binding energies of 400.2 eV and 396.9 eV assigned to N bonds in TiN and titanium oxynitrides, respectively [33,34].

The simulation of the different photoelectron spectra of Fig. 3 does not reveal unambiguously the formation of TiS in the TiN-MoS_2 thin film composites, although the S 2p photoelectron region for the sample after wear shows a small bump at the binding energy corresponding to TiS, namely 163 eV. Furthermore, peak overlapping of the TiS photoelectron signal at 163 eV in S 2p and at 454.4 eV in the Ti 2p photoelectron regions prevents a conclusive statement about the presence of TiS in the thin film composites. Nevertheless, the GIXRD analyses presented below allow us to eliminate the presence of TiS at least in the as-deposited samples.

Furthermore, there is no significant change of the XPS spectra from the TiN-MoS_2 thin film composite coatings before and after wear, especially concerning the amount of formed oxides. Thus, oxide and oxynitride formation during deposition and/or during air exposure seem to be the dominant causes for the formation of these compounds in the films.

TEM cross sections for samples 2 to 5 are shown in Fig. 4a to d. Sample 2 (Fig. 4a) presents the characteristic TiN columnar structure and some eventual, isolated MoS_2 clusters, which can be distinguished owing to the larger electronic density for MoS_2 as compared to TiN. The same behavior was found for sample 1 (not shown). Samples 3 and 4, with increasingly larger MoS_2 content, display (see Figs. 4b and c) higher concentrations of MoS_2 clusters, which are also larger in size. For these samples, the columnar structure is barely visible. A detailed TEM cross section image of sample 5 is shown in Fig. 4d, evidencing the MoS_2 clusters and the TiN matrix. The TEM images do not indicate any evidence at all of TiN-MoS_2 multilayers. The TEM cross section for sample 6 is shown in Fig. 5, where one notices clearly the nanoscopic MoS_2 clusters in the composite film, shown in better detail in the inset.

Concerning segregation of MoS_2 at grain boundaries mentioned earlier [15,16], the present TEM images do not confirm this possibility. Previous authors [15,16,22] have only shown scanning electron microscope images, which do not have enough magnification to identify these clusters. On the other hand, the present TEM images display 10 to 20 nm MoS_2 clusters homogeneously distributed in the

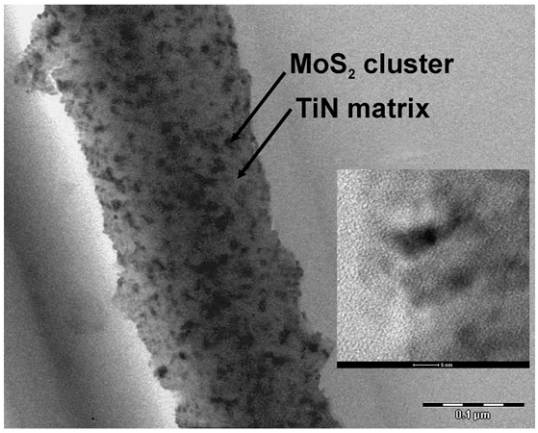

Fig. 5. Transmission electron microscopy images for MoS_2-TiN composite thin films with 40% MoS_2. The inset shows a zoom (scale is 5 nm) with details of the MoS_2 clusters in the TiN matrix.

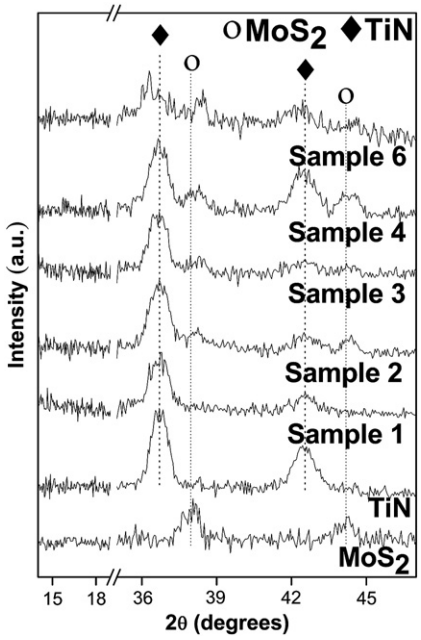

Fig. 6. Grazing incidence X-ray diffractograms for the MoS_2-TiN composite thin films of the present work. The diffractograms for MoS_2 and TiN films are also presented in the figure.

TiN matrix in all samples. Therefore, one evidences here the formation of a nanocomposite structure.

Fig. 6 shows the GIXRD results for samples 1 to 6, including pure TiN and MoS_2 thin films. It is noteworthy the absence of the basal plan MoS_2 (002) peak in the diffractograms, which has been demonstrated to depend on the specific deposition architecture and on the deposition conditions [35]. This is confirmed by the X-ray diffractogram of the sputtering target (not shown) in which this basal plan diffraction peak is the most intense one. In addition, the TiN diffraction peaks for sample 6 reveal broadening and shift to lower angles, which can be due to a reduction in grain size and to an increase in the lattice parameter, respectively. Since this was the thin film sample with the highest MoS_2/TiN ratio, this fact might indicate a competition between TiN crystalline structure and MoS_2 cluster formation.

Different authors [14–16,23] attributed the peak shifting to incorporation of sulfur substituting nitrogen in TiN lattice. This interpretation can be argued on the basis of the very large difference in ionic radii between N (0.01 nm) and S (0.184 nm), rendering this substitution very improbable. Furthermore, Ellingham diagrams for TiS and TiN show Gibbs free energy of formation equal to −115 Kcal/mol [36] and −145 Kcal/mol [37], respectively, indicating that TiN formation is much more probable than TiS in the present deposition conditions. In addition, the diffractograms do not show any peak that could be assigned to TiS. Therefore, considering the evidences of XPS and GIXRD analyses one can rule out the presence of TiS in the films.

Concerning the shift in peaks positions, a more careful analysis can be done on the basis of the GIXRD for sample 6, showed in detail in Fig. 7. Besides the shift to small angles of the TiN peaks mentioned above, Fig. 7 reveals also a shift of the MoS_2 diffraction peaks to higher 2θ values. This is indicative of a decrease in lattice parameters. Thus, probably the MoS_2 grains are submitted to compressive stress by the TiN matrix, leading the TiN grains to undergo tensile stress.

The small intensity of the MoS_2 diffraction peaks observed here is consistent with similar observations by previous authors [4,18,22,24,38,39], indicating that the majority of the MoS_2 clusters are amorphous. The present TEM images show many MoS_2 clusters with typical sizes of 20 nm embedded in the TiN matrix, without major nanocrystalline phases.

Similar to XPS analyses, no significant difference in XRD patterns could be observed before or after wear.

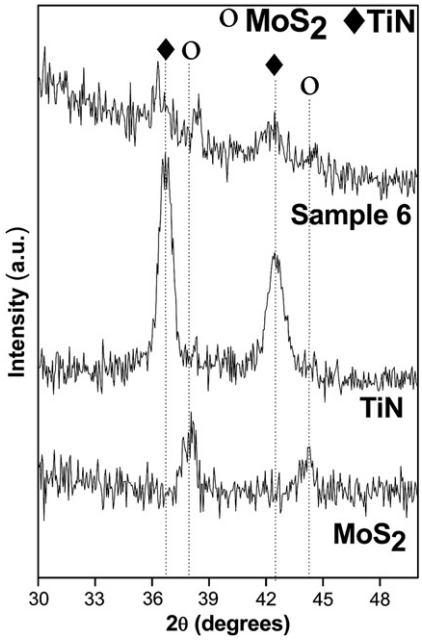

Fig. 7. Grazing incidence X-ray diffractogram for sample 6 (40% MoS_2). The shifts of the MoS_2 diffraction peaks to higher angles and of the TiN diffraction peaks to lower angles can be better visualized in this figure.

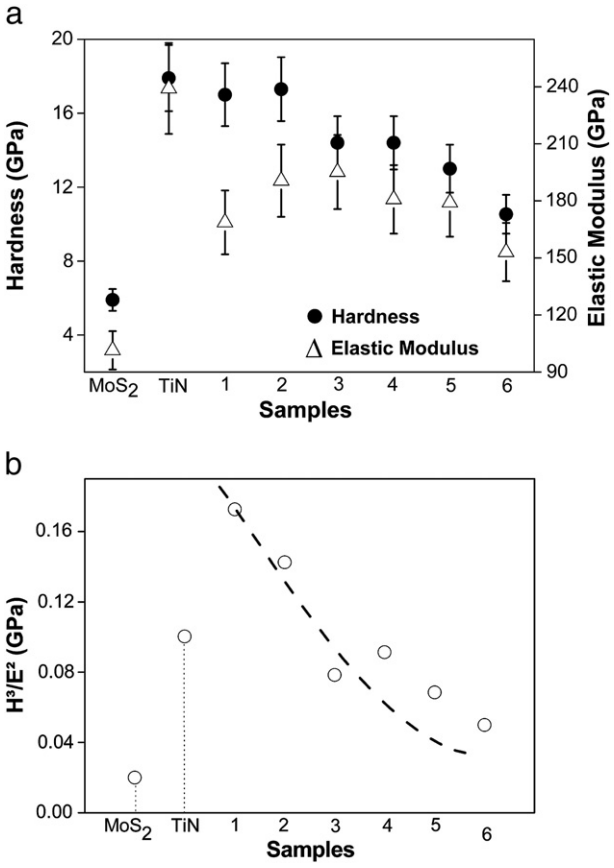

Fig. 8. (a) Hardness (full circles) and reduced elastic modulus (open triangles) for TiN, MoS_2, and for the MoS_2-TiN composite films of the present work. (b) H^3/E^2 ratio for TiN, MoS_2, and for the MoS_2-TiN composite films of the present work.

The hardness and elastic moduli of the MoS_2 and TiN films and of the different TiN-MoS_2 thin film composites were determined and the results are given in Fig. 8a. For samples 1 and 2, the hardness is roughly the same as for the pure TiN film coating, whereas for higher concentrations of MoS_2, namely samples 3 to 6 it decreases for increasing MoS_2/TiN ratio [25]. The reduced elastic modulus for sample 1, on the other hand, is substantially lower than that for TiN, increasing slightly for samples 2 and 3 and then, for higher MoS_2/TiN ratios it decreases slightly. The elastic strain to failure, or H^3/E^2 ratios, are presented in Fig. 8b, where one notices a maximum for the sample with the smallest MoS_2/TiN ratio, namely sample 1, which has 2% MoS_2. The H^3/E^2 ratio decreases somehow for sample 2 and then decreases substantially for higher values of the MoS_2/TiN ratio. We recall here the discussion of the Introduction, where it was pointed out that a high H^3/E^2 indicates a high resistance of the coating to plastic deformation and, presumably, a high wear resistance as well, besides of low stiffness.

4. Conclusions

In summary, we have studied TiN-MoS_2 composite thin films showing that: i) MoS_2 is formed in the composite during the thin film co-deposition process and not during any tribologic test procedure. Besides, MoS_2 remains like that after removal of part of the thin film by a typical dry wear process; ii) the MoS_2 clusters formed in the TiN matrix are nanoscopic in size, homogeneously distributed, and the majority of them are amorphous. However, GIXRD demonstrates that there is a minor part of nano-crystalline grains, and iii) the present XPS, TEM, and GIXRD analyses do not confirm MoS_2 formation at grain boundaries or TiS formation by substitution of S for N in the TiN matrix.

For MoS_2 concentrations up to 4%, the present TiN-MoS_2 thin film composite coatings are appreciably hard and have also appreciably high elastic strain to failure. On the other hand, the friction coefficient does not seem to depend much on the MoS_2 concentration in the interval of MoS_2 concentrations from zero to 7%. Therefore, TiN-MoS_2 thin film composites with these moderate concentrations of MoS_2 nanoclusters are potential coating materials for hardness, low friction, and wear resistance applications.

Acknowledgement

The authors would like to acknowledge CNPq for the financial support.

References

[1] C. Donnet, Surf. Coat. Technol. 80 (1996) 151.
[2] D. Bhaduri, R. Kumar, A.K. Jain, A.K. Chattopadhyay, Wear 268 (2010) 1053.
[3] M.A. Baker, R. Gilmore, C. Lenardi, W. Gissler, Appl. Surf. Sci. 150 (1999) 255.
[4] J. Haider, M. Rahman, B. Corcoran, M.S.J. Hashmi, Surf. Coat. Technol. 200 (2005) 1080.
[5] D.G. Teer, Wear 252 (2001) 1068.
[6] A. Hörling, L. Hultman, M. Odén, J. Sjölen, L. Karlsson, Surf. Coat. Technol. 191 (2005) 384.
[7] P.W. Shum, W.C. Tam, K.Y. Li, Z.F. Zhou, Y.G. Shen, Wear 257 (2004) 1030.
[8] H. Chen, J. Liu, W. Huang, Mater. Sci. Eng. A 415 (2006) 291.
[9] C. Aguzzoli, C. Marin, C.A. Figueroa, G.V. Soares, I.J.R. Baumvol, J. Appl. Phys. 107 (2010) 1.
[10] R. Gilmore, M.A. Baker, P.N. Gibson, W. Gissler, Surf. Coat. Technol. 105 (1998) 45.
[11] W.Y. Bae, Y.W. Lee, M.T. Besmann, S.C. Yust, J.P. Blau, Mater. Sci. Eng. 209 (1996) 372.
[12] I. Bertóti, M. Mohai, N.M. Renevier, E. Szilágyi, Surf. Coat. Technol. 125 (2000) 173.
[13] C. Wiemer, R. Sanjinés, F. Lévy, Surf. Coat. Technol. 86 (1996) 372.
[14] S. Gangopadhyay, R. Acharya, A.K. Chattopadhyay, S. Paul, Vacuum 84 (2010) 843.
[15] R. Goller, P. Torri, M.A. Baker, R. Gilmore, W. Gissler, Surf. Coat. Technol. 120 (1999) 453.
[16] R. Gilmore, M.A. Baker, P.N. Gibson, W. Gissler, M. Stoiber, P. Losbichler, C. Mitterer, Surf. Coat. Technol. 108 (1998) 345.
[17] N.M. Renevier, J. Hamphire, V.C. Fox, J. Witts, T. Allen, D.G. Teer, Surf. Coat. Technol. 142 (2001) 67.
[18] M. Rahman, J. Haider, D.P. Dowling, P. Duggan, M.S.J. Hashmi, Surf. Coat. Technol. 200 (2005) 1451.
[19] Y. Jing, J. Luo, S. Pang, Thin Solid Films 461 (2004) 288.
[20] K.J. Ma, C.L. Chao, D.S. Liu, Y.T. Chen, M.B. Shieh, J. Mater. Process. Technol. 127 (2002) 182.
[21] C. Piazzoni, M. Blomqvist, A. Podesta, G. Bardizza, M. Bonati, P. Piseri, P. Milani, C. Davies, P. Hatto, C. Ducati, K. Sedlackova, G. Radnoczi, Appl. Phys. A 90 (2008) 101.
[22] S. Gangopadhyay, R. Acharya, A.K. Chattopadhyay, S. Paul, Surf. Coat. Technol. 203 (2009) 3297.
[23] J. Haider, M. Rahman, J.S.M. Hashmi, Mohammed Sarwar, J. Mater. Sci. 43 (2008) 3368.
[24] X. Ding, X.T. Zeng, T. Goto, Surf. Coat. Technol. 198 (2005) 432.
[25] S. Gangopadhyay, R. Acharya, A.K. Chattopadhyay, S. Paul, Surf. Coat. Technol. 203 (2009) 1565.
[26] M.C. Simmonds, A. Savan, H. Van Swygenhoven, E. Pflüger, S. Mikhailov, Surf. Coat. Technol. 108 (1998) 340.
[27] A. Leyland, A. Matthews, Wear 246 (2000) 1.
[28] S.K. Ghosh, P.K. Limaye, B.P. Swain, N.L. Soni, R.G. Agrawal, R.O. Dusane, A.K. Grover, Surf. Coat. Technol. 201 (2007) 4609.
[29] F. Lv, S.P. Wen, R.L. Zong, F. Zeng, Y. Gao, F. Pan, Surf. Coat. Technol. 202 (2008) 3239.
[30] J. Soldán, J. Musil, Vacuum 81 (2006) 531.
[31] S. Yang, Y. Chang, D. Lin, D. Wang, W. Wu, Surf. Coat. Technol. 202 (2008) 2176.
[32] W.K. Chu, J.W. Mayer, M.A. Nicolet, Academic Press, 1978, p. 384.
[33] H. Yi, K. Dang, X. Zeng, H. Shao, T. Ren, Ind. Lubric. Tribol. 60 (2008) 79.
[34] C. Aguzzoli, E.K. Tentardini, C.A. Figueroa, C. Kwietniewski, L. Miotti, I.J.R. Baumvol, Appl. Phys. A 94 (2009) 263.
[35] E. Arslan, F. Bulbul, A. Alsaran, A. Celik, I. Efeoglu, Wear 259 (2005) 814.
[36] S.R. Shatynski, Oxid. Met. 11 (1977) 307.
[37] H.J.T. Ellingham, J. Soc. Chem. Ind. 63 (1944) 125.
[38] N.M. Renevier, N. Lobiondo, V.C. Fox, D.G. Teer, J. Hampshire, Surf. Coat. Technol. 123 (2000) 84.
[39] V. Buck, Wear 114 (1987) 263.